

Influence of the loading path on fatigue crack growth under non-proportional mixed-mode loading

V. Doquet¹, M. Abbadi, Q.H. Bui, A. Pons

¹CNRS, Laboratoire de Mécanique des Solides, Ecole Polytechnique, 91128 Palaiseau cedex, France, doquet@lms.polytechnique.fr

ABSTRACT. *Fatigue crack growth tests were performed under various mixed-mode loading paths, on a maraging steel. The effective loading paths were computed by finite element simulations, in which asperity-induced closure and friction were modelled. Application of fatigue criteria for tension or shear-dominated failure after elastic-plastic computations of stresses and strains, ahead of the crack tip, yielded predictions of the crack paths, assuming that the crack would propagate in the direction which would maximise its growth rate. This approach appears successful in most cases.*

INTRODUCTION

Under non-proportional cyclic loading, the stress or strain ranges are not sufficient to model the multiaxial cyclic behaviour of metals. Additional parameters -describing the loading path- have to be introduced into constitutive equations to capture extra-hardening effects. Concerning fatigue crack growth under non-proportional mixed-mode, a similar question arises: are ΔK_I , ΔK_{II} sufficient to predict crack paths and growth rates? Does the loading path have an *intrinsic* influence, or can all this influence be captured through appropriate corrections for closure and friction effects on stress intensity factors?

To investigate this question, crack growth tests were performed under various mixed-mode loading paths, to compare the crack paths. Elastic and elastic-plastic finite element (FE) simulations -in which asperity-induced closure and friction are modelled- were used to analyze the influence of the loading path and predict the crack path.

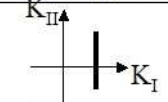
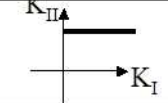
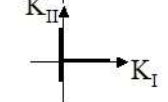
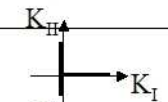
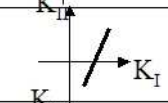
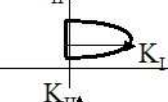
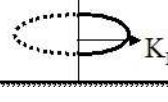
EXPERIMENTS

Procedures

The material investigated is a maraging steel, for which kinetic data concerning mode II fatigue crack growth is available from a previous study [1]. It has a very high yield stress ($R_{p0.2} \approx 1720$ Mpa) but very low hardening capacity ($R_m/R_{p0.2} \approx 1.03$) and limited ductility (around 8%). Tubular specimens (10.8mm and 9mm outer and inner diameters)

were used for push-pull, reversed torsion and reversed torsion plus static tension tests, in order to fit constitutive equations and two fatigue criteria: one for shear-dominated failure –which occurred systematically in torsion- (Findley’s criterion [2]) and one for tension-dominated failure which occurred in push-pull (Smith, Watson and Topper’s criterion [3]). This preliminary part of the study is reported in appendix.

Table 1: Test conditions, observed and predicted crack paths

Loading path	ref	Loading parameters	Measured bifurcation angle	Predicted bifurcation angle
	A	$\Delta K_{II}=20\text{MPa}\sqrt{\text{m}}, K_I=7.5\text{MPa}\sqrt{\text{m}}$ $\Delta K_{II}=20\text{MPa}\sqrt{\text{m}}, K_I=10\text{MPa}\sqrt{\text{m}}$ $\Delta K_{II}=20\text{MPa}\sqrt{\text{m}}, K_I=13\text{MPa}\sqrt{\text{m}}$	0 0 0	0 0 0
	B	$\Delta K_I=15\text{MPa}\sqrt{\text{m}}, K_{II}=10\text{MPa}\sqrt{\text{m}}$	$< 4^\circ$	0
	C ₁	$\Delta K_I=5.6\text{MPa}\sqrt{\text{m}}, \Delta K_{II}=20\text{MPa}\sqrt{\text{m}}$ $\Delta K_I=1.1\text{MPa}\sqrt{\text{m}}, \Delta K_{II}=20\text{MPa}\sqrt{\text{m}}$ $\Delta K_I=16.4\text{MPa}\sqrt{\text{m}}, \Delta K_{II}=20\text{MPa}\sqrt{\text{m}}$ $\Delta K_I=2.1\text{MPa}\sqrt{\text{m}}, \Delta K_{II}=20\text{MPa}\sqrt{\text{m}}$ $\Delta K_I=2.6\text{MPa}\sqrt{\text{m}}, \Delta K_{II}=20\text{MPa}\sqrt{\text{m}}$	0 0 0 0 $<4^\circ$	0 0 0 0 0
	C ₂	$\Delta K_I=1.6\text{MPa}\sqrt{\text{m}}, \Delta K_{II}=3.0\text{MPa}\sqrt{\text{m}}$ $\Delta K_I=23.7\text{MPa}\sqrt{\text{m}}, \Delta K_{II}=3.0\text{MPa}\sqrt{\text{m}}$ $\Delta K_I=3.2\text{MPa}\sqrt{\text{m}}, \Delta K_{II}=3.0\text{MPa}\sqrt{\text{m}}$	0 0 $<4^\circ$	0 0 0
	D	$\Delta K_I=10\text{MPa}\sqrt{\text{m}}, \Delta K_{II}=20\text{MPa}\sqrt{\text{m}}$	0° for $80\mu\text{m}$ then 30°	0
	E	$\Delta K_I=7.5\text{MPa}\sqrt{\text{m}}, \Delta K_{II}=20\text{MPa}\sqrt{\text{m}}$ $\Delta K_I=10\text{MPa}\sqrt{\text{m}}, \Delta K_{II}=20\text{MPa}\sqrt{\text{m}}$	0 0	0 0
	F	$\Delta K_I=7.8\text{MPa}\sqrt{\text{m}}, \Delta K_{II}=20\text{MPa}\sqrt{\text{m}}$ $\Delta K_I=10.6\text{MPa}\sqrt{\text{m}}, \Delta K_{II}=20\text{MPa}\sqrt{\text{m}}$ $\Delta K_I=1.6\text{MPa}\sqrt{\text{m}}, \Delta K_{II}=20\text{MPa}\sqrt{\text{m}}$	0 0 50	0 0 0

Some tubular specimens had a circular hole ($370\mu\text{m}$ in diameter) from which a 1 to 1.5mm-long transverse precrack was grown in mode I. The precracked specimens were submitted to tension and torsion cyclic loadings, following various loading paths (Table 1). Loading E and F, which both appear as truncated ellipses in K_I - K_{II} plane, correspond to 90° out-of-phase tension and shear, but in the first case, loading is fully reversed, while in the second case, only shear-mode loading is reversed, but $R=0$ for mode I.

Nominal and effective loading paths

$K_I^{\text{nominal}}, K_{II}^{\text{nominal}}$ were computed for a crack emanating from a hole in a infinite plate, but corrections were applied to take into account the influence of the curvature of the tube wall, which, according to Erdogan and Ratwani increases as the crack grows [4]. Finite element simulations of applied loadings were performed with rough crack faces (Figure 1), taking into account the contact and friction of the asperities. A sine wave

profile with amplitude h -ranging from 5 to 20 μm - and period p -around 180 μm - was assumed, which is simplified, but reasonable compared to observed precrack profiles. The effective stress intensity factors, $K_I^{\text{effective}}$, $K_{II}^{\text{effective}}$, were computed at each time step (by analysis of crack faces displacements). Plasticity-induced closure –probably limited in such a high strength steel- was not taken into account.

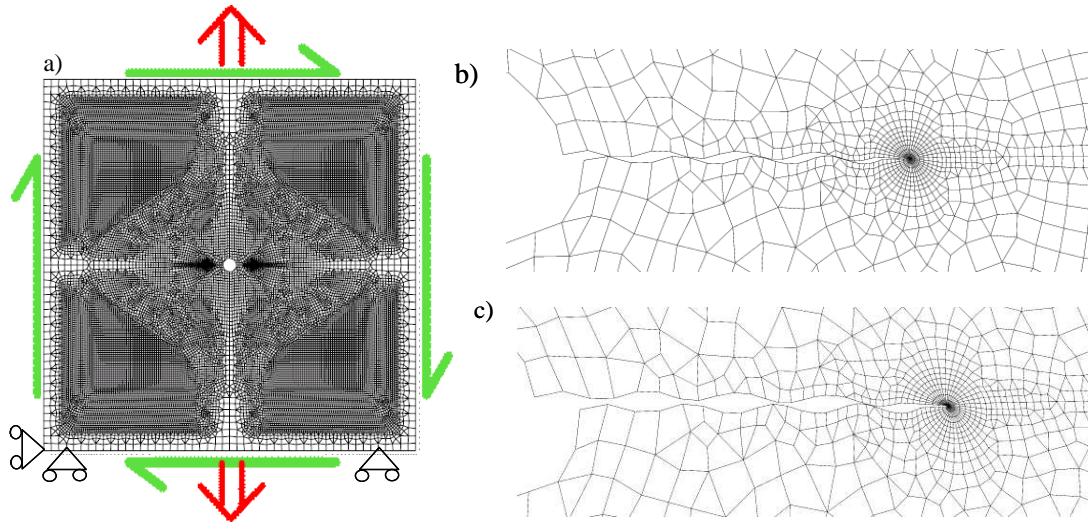


Figure 1: Finite element model for the computation of effective loading paths. a) mesh and boundary conditions, b) and c) deformed mesh for two levels of applied shear.

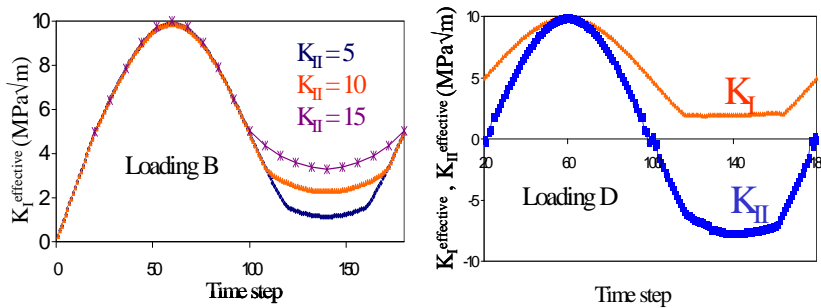


Figure 2: Computed evolutions of effective stress intensity factors for loading B and D.

As an example, figure 2 shows the evolutions in time of effective stress intensity factors computed for loading B and D, with $h=10\mu\text{m}$ and friction coefficient $\mu=1$. Figure 3 shows the mutual influence of each mode on the effective stress intensity factor of the other mode for $\Delta K_I=10\text{Mpa}\sqrt{\text{m}}$ and $\Delta K_{II}=20\text{Mpa}\sqrt{\text{m}}$. Important asperity-induced closure - increasing with K_{II} - was found for cyclic mode I plus static mode II. Closure effect were found less important for mixed-mode plus static mode I and absent for all other investigated loading paths. A static mode I or a cyclic, 90° out-of-phase mode I, were found to reduce crack tip shielding from mode II loading by crack faces interactions, compared to pure mode II, while in-phase mode I cyclic loading, with $R=-$

1 was found to enhance it. Very limited influence of mode I on $\Delta K_{II}^{\text{effective}}$ was found here for sequential loading, but simulations performed for $\Delta K_I=15\text{MPa}\sqrt{\text{m}}$, $\Delta K_{II}=20\text{MPa}\sqrt{\text{m}}$ for a much softer ferritic-pearlitic steel in a previous study [5] have shown that for such loading, the residual crack tip opening increases from cycle to cycle. This effect, which would probably be observed in maraging steel at higher ΔK_I is likely to reduce crack faces interference and increase $\Delta K_{II}^{\text{effective}}$.

Note that for similar nominal loading ranges, $\Delta K_I=10\text{MPa}\sqrt{\text{m}}$ and $\Delta K_{II}=20\text{MPa}\sqrt{\text{m}}$, variations in the loading path lead to variations in $\Delta K_I^{\text{effective}}$ from 7.9 to $10\text{MPa}\sqrt{\text{m}}$ and in $\Delta K_{II}^{\text{effective}}$ from 11.1 to $20\text{MPa}\sqrt{\text{m}}$! Such differences in effective loading can produce differences in crack paths and growth rates.

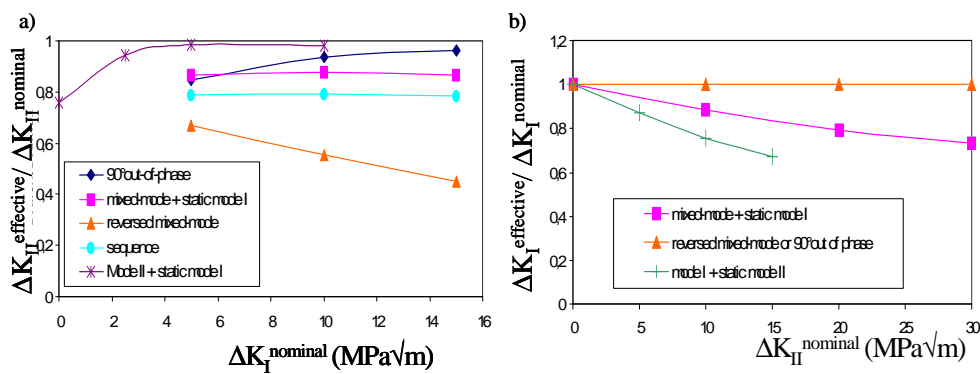


Figure 3: Mutual influence of mode I and mode II on the effective fraction of ΔK of the other mode ($h=10\mu\text{m}$, $p=180\mu\text{m}$) a) $\Delta K_{II}=20\text{MPa}\sqrt{\text{m}}$ and b) $\Delta K_I=10\text{MPa}\sqrt{\text{m}}$.

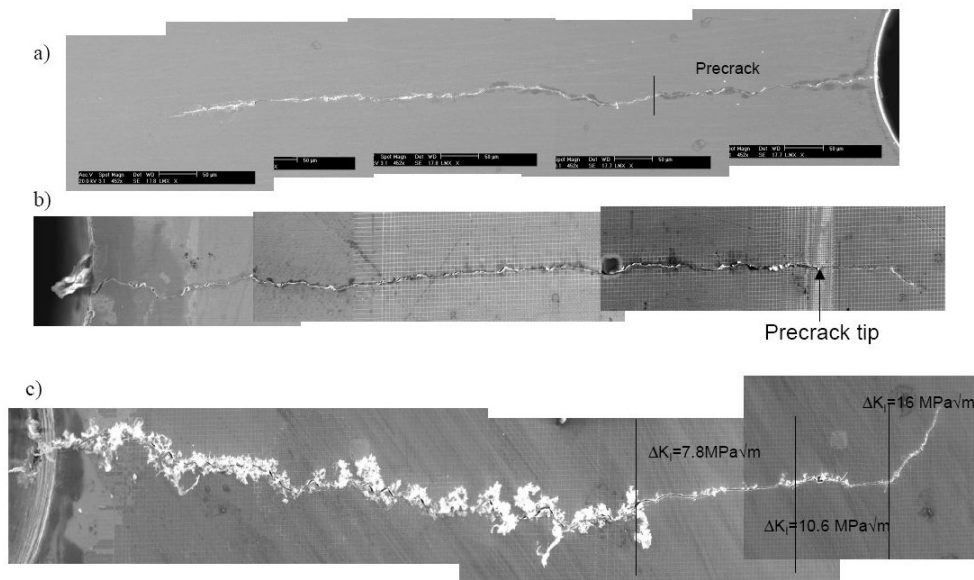


Figure 4: crack paths for a) sequential mixed-mode loading (C1) b) in-phase mixed-mode + static mode I (D) c) fully reversed 90° out-of-phase mixed-mode (F).

Observed crack paths

Table 1 summarises the observations, concerning the crack paths. Pictures of crack paths after loading C₁, D and F are shown on figure 4. Crack growth was nearly coplanar for sequential loading C₁ and C₂. The slight deflections observed during the final blocks of these tests seem not to be due to the applied mixed-mode, but to incipient shear-lips, due to the relatively high ΔK_I . Loading D (in phase mixed-mode plus static mode I) lead to 80 μ m coplanar crack growth, followed by bifurcation at 30°. Coplanar crack growth was observed, during the first and second block of fully reversed, 90° out-of-phase loading F. Bifurcation at 50° occurred during the third block. A large quantity of fretting debris appeared along the rough precrack, but much less along the smoother coplanar crack part, grown in mixed-mode. By contrast, only coplanar crack growth was observed for path E (also 90° out-of-phase, but R=0 for mode I). Much less fretting debris was formed and the fracture surfaces were not mated, contrary to the previous case. This might partly be due to a smoother precrack, but mainly to the absence of compressive loading while shearing is being applied.

ANALYSIS

Elastic-plastic FE simulations of applied loadings were performed for rough crack faces, using constitutive equations with isotropic and non-linear kinematic hardening fitted to measured stress-strain curves. Findley's damage function was computed ahead of the crack tip and averaged along the radial segment of length l ($l=20\mu$ m in the computations reported below) for which the shear stress range was maximum, whereas for the computation and averaging of Smith-Watson-Topper's damage function, two choices of critical plane were envisaged: the planes along which either the peak normal stress, σ_{nmax} , or the normal stress range $\Delta\sigma_n$ were maximum. These two cases, which can yield very different predictions, as shown below, will be denoted by SWTa and SWTb. These two potential growth directions were envisaged by Hourlier et al [6] and Dahlin and Olsson [7]. The former concluded that the direction of maximum $\Delta\sigma_n$ was more suitable for alloys showing a limited influence of the R ratio on their mode I kinetics, which is the case of the maraging steel investigated here. The latter concluded that the direction of maximum σ_{nmax} should be preferred for high-strength metals with limited ductility, which is also the case of the maraging steel investigated here!

The analysis of the crack path for cyclic mode I + static mode II (test B) is very useful to solve that dilemma. For these loading conditions, the peak σ_{nmax} occurs at 62° while the maximum $\Delta\sigma_n$ is at 0°, whatever the static mode II. Since no bifurcation occurred, the crack followed the maximum $\Delta\sigma_n$ plane. SWTb criterion was thus used for tension-dominated failure and Findley's criterion, for shear-dominated failure.

The potential numbers of cycles to fracture $N_f(l)$ are computed, using the analytical relations between damage functions and fatigue lives, fitted to experimental data on smooth specimens (see appendix). The crack is supposed to grow in the direction where failure – be it tension or shear-dominated- occurs first or, in other words, in the

direction where its growth rate is maximum. This generalises the idea of Hourlier et al [6] who promoted it, under the restrictive assumption that mode I would necessary prevail. The potential growth rates in corresponding directions are then estimated as:

$$\frac{da}{dN} \approx \frac{l}{N_f(l)} \quad (1)$$

Prediction of crack path and growth rate in fully reversed mode II

Figure 5 compares the potential crack growth rate in fully reversed mode II predicted by Findley’s criterion and that of a branch crack, in mode I, according to SWTb for various amplitudes. These computations were performed for a smooth, frictionless crack. Coplanar growth is predicted for $\Delta K_{II}^{effective}$ higher than 15MPa√m, which is consistent with the threshold found by Pinna [1]. The predicted mode II crack growth rate is correct above 25MPa√m, but a bit too small below that value. This can be improved by introducing a damage cumulation, to take into account the smaller cycles before the crack tip touches the element whose fatigue life is computed. This will be reported elsewhere, for lack of space.

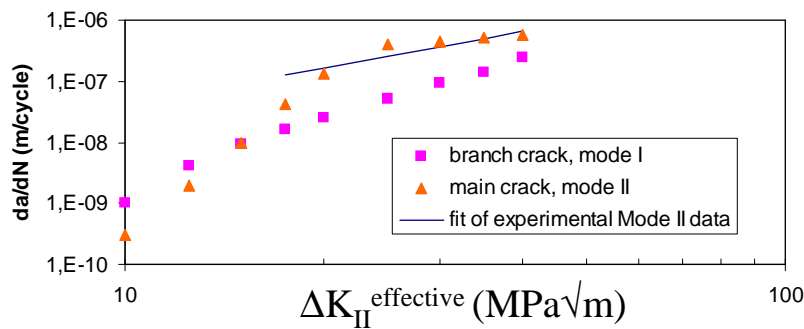


Figure 5: Potential crack growth rate in reversed mode II predicted by Findley’s criterion and that of a branch crack, in mode I, according to SWTb.

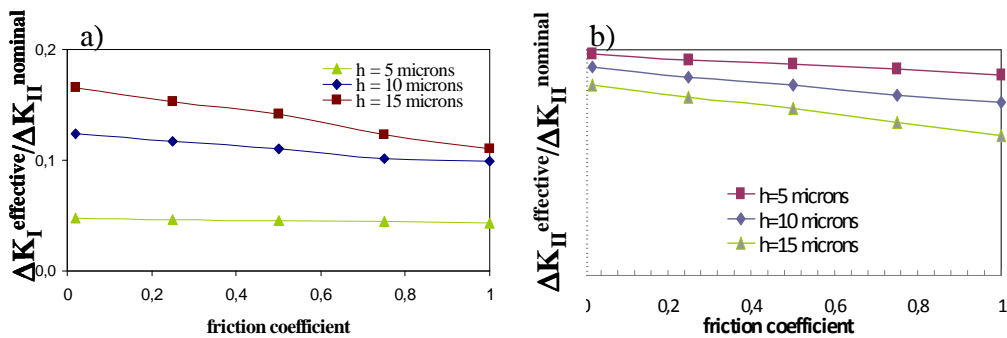


Figure 6: Influence of crack roughness and friction coefficient on a) $\Delta K_I^{effective}$ and b) $\Delta K_{II}^{effective}$ in reversed mode II.

Simulations of reversed mode II were performed for a rough crack, with $h=5, 10$ and $15\mu\text{m}$ and friction coefficients, μ , between 0 and 1 (Figure 6). The higher μ , the smaller $\Delta K_{II}^{\text{effective}}$. Mode I induced by asperities is predicted to increase and $\Delta K_{II}^{\text{effective}}$ to decrease with h , so that for $\Delta K_{II}=20\text{Mpa}\sqrt{\text{m}}$, coplanar growth is predicted for $h=5$ and $10\mu\text{m}$, whatever the friction coefficient, and for $h=20\mu\text{m}$, only if μ is smaller than 0.44, while bifurcation is predicted above this value. Slight changes in crack roughness or tribological conditions are thus likely to change the crack paths. Mode II crack growth is favoured by smooth crack faces and a low friction coefficient.

Prediction of crack paths in non-proportionnal mixed-mode

The predicted crack paths for mixed-mode loadings A to F reported in Table 1 were obtained for $h=10\mu\text{m}$ and $\mu=1$. In most cases, it is in agreement with the observed crack paths, but some discrepancies exist. The final bifurcation at 30° , observed after coplanar growth during test D and the bifurcation at 50° during the last block of tests F are not predicted. Since it proved difficult to control at the same time the symmetry of precracking on each side of the hole, the final length of precracks and their roughness, differences from specimen to specimen might be responsible for the few mispredictions, not to mention three-dimensional aspects that will be addressed in a next step.

CONCLUSIONS

Finite element simulations of crack faces interactions show that for fixed nominal loading ranges, variations in the loading path, crack roughness or friction coefficient induce important variations in $\Delta K_I^{\text{effective}}$ and $\Delta K_{II}^{\text{effective}}$ likely to change the crack path. An approach based on elastic-plastic FE computations and local application of fatigue criteria was developed to analyze the crack paths observed during mixed-mode experiments on a maraging steel. The predictions were successful in most cases.

APPENDIX: Fit of fatigue criteria

Tension-dominated failure which occurs in push-pull can be predicted with Smith, Watson and Topper's criterion [3] in which the damage parameter is

$$\beta_{SWT} = \Delta \varepsilon_n \sigma_{n \max} \quad (\text{A1})$$

Figure A1a shows the measured fatigue lives in push-pull or repeated tension as a function of β_{SWT} . An exponential law was fitted and used for crack growth predictions.

Shear-initiated decohesion along a slip band in fatigue occurs earlier when an opening stress is present. Findley [2] took this effect into account in a crack initiation criterion where the damage function:

$$\beta_{Find} = \Delta\tau + k\sigma_{n\max} \quad (\text{A2})$$

incorporates the peak opening stress $\sigma_{n\max}$, computed along the facet which undergoes the maximum shear stress range, $\Delta\tau$. Figure A1b shows the measured fatigue lives in reversed torsion with various static tensile stresses as a function of β_{SWT} in which $k=0.2$ gave the best correlation. There again an exponential fit was obtained.

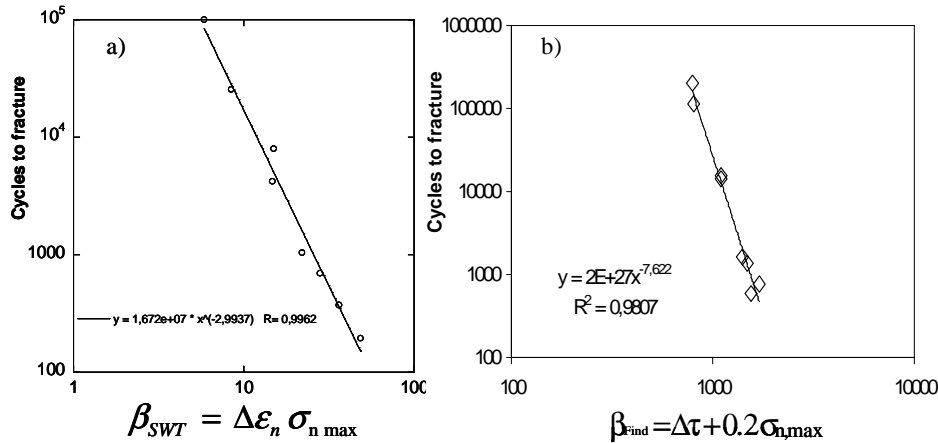


Figure A1: Fit of a) Smith, Watson and Topper's fatigue criterion from tensile fatigue data and b) Findley's criterion from reversed torsion + static tension data.

Acknowledgments : This study was supported by the Agence Nationale de la Recherche

REFERENCES

1. Pinna C., Doquet V. (1999), *Fat. Fract. Eng. Mat. Struct* **22**, 173-183.
2. Findley W.N. (1957), *Trans ASME* **79**, 1337-1348.
3. Smith K.N., Watson P. and Topper T.H. (1970), *Journal of materials* **5**, 767-778.
4. Erdogan F., Ratwani M. (1972), *Int. Journ. Fract. Mech* **8**, 87-95.
5. Doquet V., Pommier S. (2004), *Fat. Fract. Eng. Mat. Struct* **27**, 1051-1060.
6. Hourlier F., d'Hondt H., Truchon M., Pineau A. (1985), *Multiaxial Fatigue*, ASTM STP 853, KJ Miller and MW Brown eds, ASTM, Philadelphia, 228-248.
7. Dahlin P., Olsson M. (2003), *Fat. Fract. Eng. Mat. Struct* **26**, 577-588.